Continuously observing the spectrum of a dynamically decoupled spin-1 quantum gas

R. P. Anderson,[1] M. J. Kewming,[1] and L. D. Turner[1]

[1] *School of Physics & Astronomy, Monash University, Victoria 3800, Australia.*

(Dated: June 14, 2017)

Quantum states and spectra can be made sensitive to a particular measurand whilst simultaneously impervious to parasitic fluctuations of an environment. Here we use an atom-light interface with minimal backaction to probe the spectrum of a radiofrequency-dressed spin-1 quantum gas continuously and in-situ. The dressing amplitude sets the radiofrequency band in which oscillating magnetic fields manifest a linear measurand, and we probe the energy spectrum and coupling strengths during unitary evolution of the system. By varying a symmetry-breaking parameter of the Hamiltonian, we find a regime in which two of the dressed states are maximally insensitive (up to fourth-order) in magnetic field fluctuations that are slow compared to the dressed-state splittings. Moreover, we demonstrate the predictive power of our continuous probe to optimize the dynamical decoupling and tune the measurement band. This robust system shares the useful hallmarks of quantum metrology platforms; the states are thus termed "synthetic clock" states in a complementary result by Lundblad et al. (arXiv:1706.xxxx) and are candidates for band-tunable magnetometry and emulation of quantum magnetism in solid-state systems.

From Hahn echoes to contemporary dynamical decoupling, abrupt, discrete rotations have been used to protect spin superpositions from inhomogeneities and parasitic fluctuations, prolonging quantum coherence and circumventing deleterious energy shifts [1–3]. A complementary strategy is to replace the pulse train with an uninterrupted coupling of 'bare' spin states, thus admitting new 'dressed' spin eigenstates, with a modified quantization direction, spectrum, and coupling, which too are protected from unwanted artifacts of their environment [4]. This *continuous* dynamical decoupling (CoDD) has proven useful across multiple platforms including nitrogen-vacancy centers [5–8] and superconducting qubits, and forms the basis for creating protected qubit [9] and decoherence-free [10] subspaces. Weak continuous measurement is a powerful instrument for appraising and refining dynamical decoupling in real time; to probe stochastic evolution, improve metrological bandwidth, or realize quantum feedback schemes [11]. Here we use dispersive optical readout of a 'bare' spin component $\hat{F}_x$ to measure the spectrum of a continuously decoupled spin-1 quantum gas using time-resolved Fourier spectroscopy. Fourier transform spectroscopy has been to measure band structures of a spin-orbit coupled BEC [12] by composing multiple non-contiguous projective measurements. The rich time-frequency domain data in our experiment reveal not only multiple dressed-state splittings and their relative immunity to noise, but also dressed state coherences and coupling strengths. This potent ability to estimate the eigenspectrum of a multilevel dressed system reveals features absent in spin-1/2 or composite spin-1/2 qubit systems; principally, we identify a regime in which a subspace of the dressed system is maximally decoupled from noise $\propto \hat{F}_z$. This subspace is spanned by two of the dressed states, termed 'synthetic clock states' in a co-submission by Lundblad et al. (arXiv:1706.xxxx). The low-frequency magnetic stability and high-bandwidth detection of these states is immediately applicable to band-tunable (ac) magnetometry [5, 6, 13] and experiments preparing delicate spin-entangled many-body states [14]; whereas the unconventional cyclic coupling of all $2F+1$ dressed states could be applied to emulation of frustrated quantum spin chains [15].

Atomic Zeeman states $|m_z = -1, 0, 1\rangle$ in a magnetic field $B_z\mathbf{e}_z$ can be decoupled from fluctuations in B_z by applying a perendicular radiofrequency (rf) field $B_{\rm rf}\mathbf{e}_x \cos\omega_{\rm rf}t$, oscillating at $\omega_{\rm rf}$, tuned near the splitting of the Larmor frequency $\omega_L \equiv (E_{m_z=+1} - E_{m_z=-1})/2\hbar$. At low magnetic fields, the degeneracy of the composite spin-1/2 systems [16] renders the spin-1 behavior identical to CoDD in spin-1/2 systems. In the dressed-state picture, the spin is quantized along x in a frame rotating with the radiofrequency $\omega_{\rm rf}$, i.e. the eigenstates of $\mathcal{H}_{\rm rwa} = \Delta\hat{F}_z + \Omega\hat{F}_x$ are $|m_x = -1, 0, 1\rangle$, with energies $m_x\hbar\sqrt{\Omega^2+\Delta^2}$, where $\Delta = \omega_{\rm rf} - \omega_L$ is the detuning and $\Omega = \gamma B_{\rm rf}/2$ is the Rabi frequency. Radiofrequency dressing induces an avoided crossing in the dressed energy spectrum, at resonance $\Delta = 0$ reducing the leading-order sensitivity of the 'bare' state energies ($\omega_L \approx \gamma B_z$ where γ is the gyromagnetic ratio) to magnetic field variations δB_z from linear to merely quadratic sensitivity. The spin character and symmetries are otherwise unchanged: transverse magnetic fields oscillating near the splitting frequencies drive transitions between eigenstates. In the dressed system this means relatively low-frequency ('ac') fields oscillating near the Rabi frequency Ω, such as $B_{\rm y,ac}\mathbf{e}_y \cos\Omega t$ and $B_{\rm z,ac}\mathbf{e}_z \cos\Omega t$, drive transitions $|m_x = -1\rangle \leftrightarrow |m_x = 0\rangle$ and $|m_x = 0\rangle \leftrightarrow |m_x = +1\rangle$. This is the basis for ac magnetometry [5] of relatively low-frequency fields; and for concatenated CoDD which protects against fluctuations in Ω [7]. Insensitivity to wider bandwidth and larger amplitude δB_z can be achieved by increasing Ω, opening a broader gap

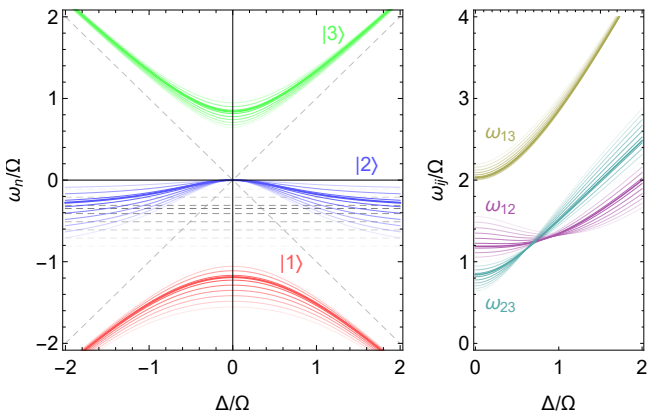

FIG. 1. Energy spectrum and splittings of a radiofrequency coupled spin-1 for various $q \in [0, \Omega]$. The transparency of each curve is proportional to the distance of q/Ω from $q_{R,\mathrm{magic}}$ in Eq. (1). (Left) Energies ω_n of dressed states $|n\rangle = |1\rangle$, (red) $|2\rangle$ (blue), and $|3\rangle$ (green) normalized to the rf-coupling strength (Rabi frequency) Ω as a function of detuning $\Delta = \omega_{\mathrm{rf}} - \omega_L$, Dashed lines indicate the energies of uncoupled states ($\Omega = 0$) in a frame rotating at ω_{rf}. (Right) Splittings ω_{ij} of dressed states $|i\rangle$ and $|j\rangle$ as a function of detuning. When $q/\Omega = q_{R,\mathrm{magic}}$ (bold curves), energies ω_1 and ω_2 share the same curvature, and their difference ω_{12} (right, purple) is minimally sensitive to detuning and thus magnetic field variations.

in the dressed spectrum, but doing so changes the detection band of the exquisitely sensitive quantum lock-in detection recently demonstrated using NV centers [17]. Henceforth we presume Ω is fixed by the application.

Any $\hat{F}_z^2$ interaction – arising from nonlinear Zeeman [18], microwave ac-Stark [19], or tensor light [20] shifts – raises the degeneracy of the $|m_z = -1\rangle \leftrightarrow |m_z = 0\rangle$ and $|m_z = 0\rangle \leftrightarrow |m_z = +1\rangle$ transitions, and breaks the symmetry of $\mathcal{H}_{\mathrm{rwa}} = \Delta\hat{F}_z + \Omega\hat{F}_x + q\hat{F}_z^2$, where $q \equiv (E_{m_z=+1} + E_{m_z=-1} - 2E_{m_z=0})_{\Omega=0}/2\hbar$. This yields dressed eigenstates $\{|1\rangle, |2\rangle, |3\rangle\}$ that are no longer SO(3) rotations of the bare Zeeman states $|m_z\rangle$, but have nematic order [LDT: $|m_z = 0\rangle$ is nematic!], and an eigenspectrum $\omega_i(\Delta) = E_{|i\rangle}/\hbar$ shown in Fig. 1 (left).Moreover, the couplings between these dressed states are markedly different: the spin operators $\hat{F}_{x,y,z}$ [Susbcript for dressed operators?] in the dressed basis span more of SU(3) for $q \neq 0$. The matrix element $\langle i|\hat{F}_x|j\rangle$ is non-zero for all i, j signifying direct coupling of dressed states $|1\rangle$ and $|3\rangle$, in contrast to the bare states where only adjacent states are coupled. Just as for bare states, we can characterize the splittings [we are using splittings and transitions around here...] between dressed states near $\Delta = 0$ as arising from a dressed Larmor frequency $\omega_D \equiv (\omega_3 - \omega_1)/2 = \sqrt{\Omega^2 + q_D^2}$, and dressed quadratic shift $q_D \equiv (\omega_3 + \omega_1 - 2\omega_2)/2 = -q/2$, giving splittings $\omega_{23} = \omega_D - q_D$, $\omega_{12} = \omega_D + q_D$ and $\omega_{13} = 2\omega_D$.

A figure-of-merit for decoupling is the curvature of the transition frequency at resonance. In a dressed two-level system there is one convex and one concave eigenstate and splitting is simply convex. Figure 1 shows that in our three-level system with quadratic shift, two states are convex. At a particular value of the normalized quadratic shift $q_R = q/\Omega$ the curvature is equal for $|1\rangle$ and $|2\rangle$ and the curvature of ω_{12} vanishes. This 'magic' value is [21]

$$q_{R,\mathrm{magic}} = \sqrt{(3\sqrt{2} - 4)/2} \approx 0.348. \quad (1)$$

resulting in vanishing quadratic dependence of their transition frequency $\omega_{12} = \omega_2 - \omega_1$ on Δ [22]. The leading-order sensitivity of these states to field variations δB_z at $q_{R,\mathrm{magic}}$ is quartic [23], giving the subspace comprised of $|1\rangle, |2\rangle$ a higher-order decoupling than can be achieved with a two-level system; [... or similar bombastic sentence. This needs oomph.] [Need to decide on spin-1/2 versus two-level etc.] we join Lundblad et al. in terming these 'synthetic clock states'.

We optimise of this high-order decoupling in the laboratory with a continuous measurement of the dressed spectrum of a spin-1 non-degenerate quantum gas. Using a single realisation of the quantum gas, we adiabatically increase the detuning from resonance making many successive measurements, each of which simultaneously measures all three splittings ω_{ij} between the dressed states. Our spinor quantum gas apparatus [24] and Faraday atom-light interface [25] are described elsewhere. We prepare an ultracold gas ($\sim 1\,\mu$K) of approximately 10^6 ^{87}Rb atoms in a crossed-beam optical dipole trap. A radiofrequency field of amplitude $\Omega/(2\pi) \leq 100\,$kHz couples the three Zeeman states $|m_z = -1, 0, +1\rangle$ of the lowest hyperfine ground state. To perform a weak measurement of the evolving spin, we focus a linearly polarized far-off-resonant probe beam ($\lambda = 781\,nm$) onto the atoms. The spin component Larmor precessing transverse to the constant magnetic bias field rotates the polarization of the probe via the paramagnetic Faraday effect; shot-noise limited polarimetry reveals $\langle\hat{F}_x\rangle$ as an modulated tone near ω_{rf}. Similar weak continuous measurements using the paramagnetic Faraday effect have been used to observe spin-mixing dynamics of a polar spinor condensate [26] and perform quantum state tomography [20, 26].

To probe the dressed state spectrum and coherences, we prepare a superposition of dressed states by suddenly turning on the Rabi coupling Ω at $t = 0$, projecting the polarized collective spin $|m_z = -1\rangle$ onto $|\psi(t = 0)\rangle = \sum_i c_i|i\rangle$. The total magnetic field in the laboratory frame used to affect this control is $\mathbf{B}(t \geq 0) = -B_{\mathrm{rf}}\cos(\omega_{\mathrm{rf}}t)\mathbf{e}_x + B_z(t)\mathbf{e}_z$, where $B_z(t)$ varies slowly compared to Ω. The resulting Faraday signal is presented in the time-frequency domain using the short-time Fourier transform (spectrogram), revealing the rich frequency and amplitude modulation related to the dressed state energies, coherences, and coupling strengths. For

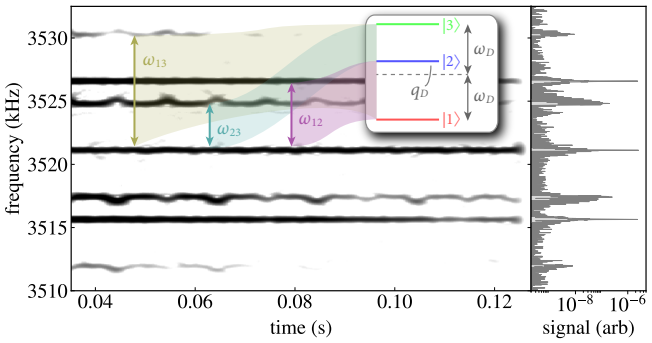

FIG. 2. Continuous measurement of the dressed energy spectrum for $q_R = 0.402(3)$, $f_{\rm rf} = 3.521\,\text{MHz}$ and $B_0 = 5.013\,\text{G}$ (left) and a periodogram of the 100 ms long signal (right). (Inset) The dressed state energy diagram for resonant coupling ($|\Delta| \ll \Omega$); the mean and difference of transition frequencies ω_{12} and ω_{23} is the dressed Larmor frequency ω_D and quadratic shift q_D, respectively. The upper sidebands about the carrier at $f_{\rm rf}$ are associated with the ω_{13} (gold), ω_{23} (turquoise), and ω_{12} (lavender) transitions. Magnetic field fluctuations $\delta B_z = \delta B_{\rm ac}(t)$ of amplitude 1.4 mG induced by mains power are manifest as asymmetric frequency modulation of the ω_{13} and ω_{23} sidebands, while the ω_{12} transition remains relatively unaffected. The corresponding spectral peaks have linewidths 102 Hz, 97 Hz, and 24 Hz, respectively. The ω_{12} linewidth is transform-limited, whereas the broadened peaks of the less decoupled ω_{23} transition exhibit a skew (third-moment) of 84 Hz (upper sideband) and −100 Hz (lower sideband).

example, with no deliberate variation of the Rabi frequency or detuning, we observe the spectrogram amplitude shown in Fig. 2. Strong amplitude modulation of the Faraday signal is apparent from the three upper and lower sidebands, each pair equidistant from the carrier frequency at $f_{\rm rf} = \omega_{\rm rf}/(2\pi)$. Each pair of sidebands corresponds to a dressed state transition $|i\rangle \leftrightarrow |j\rangle$; with sideband frequencies $f_{\rm rf} \pm f_{ij}$ where $f_{ij} = \omega_{ij}/(2\pi)$. In this way, the spectrogram is a calibration-free, real-time measurement of the dressed state spectrum. Restricting attention to the upper sidebands, the two closest to the carrier are adjacent state transitions ω_{12} and ω_{23} with similar amplitudes and with frequency separations $\omega_D \pm q_D$ from the carrier for near-resonant coupling of the bare Zeeman states ($|\Delta| \ll \Omega$). The third, weaker sideband near $2\omega_D$ above the carrier signifies the cyclic $|1\rangle \leftrightarrow |3\rangle$ transition, appearing when $q \neq 0$. No attempt was made to shield the apparatus from parasitic magnetic fields. Power line magnetic field noise causes a temporally varying $\delta B_z = \delta B_{\rm line}(t)$ at the line frequency of 50 Hz and its odd harmonics, of $\sim$ 1.4 mG (1 kHz) peak-to-peak. For these data $q_R = 0.402(3)$, and each dressed transition is affected by the magnetic fluctuations differently: the sidebands corresponding to the ω_{13} and ω_{23} transitions exhibit asymmetric frequency modulation, whereas the optimally decoupled ω_{12} transition remains unperturbed within the frequency resolution of this spectrogram. A periodogram (Fig. 2, right) of the entire time-series yields maximum frequency resolution (at the expense of all temporal resolution) shows the outwardly-skewed peaks expected for transitions convex in Δ, e.g. the ω_{23} sidebands have a substantial third moments [Are we sure units of third moments are Hz not Hz^3?] and a second moment (standard deviation) that is 4 times broader than the transform-limited [no, transform limited should be a few Hz only!] peak of the ω_{12} transition (24 Hz second-moment).

The amplitude of each sideband is proportional to the corresponding dressed-state coherence $\rho_{ij} = c_i^* c_j$, and to the dressed state coupling strength induced by the relevant spin projection operator $\hat{F}_{x,y,z}$ [Which is relevant to us? How do I know?]. An analytic expression for coupling amplitudes near resonance ($\Delta \ll \Omega$) is summarized in Table I. These depend on the initial projection onto the dressed basis, which if known amounts to continuous measurement of all coupling strengths in the dressed basis, effecting Hamiltonian parameter estimation for the dressed-system couplings [process tomography/ Hamiltonian learning]. Alternatively, if the dressed state couplings are separately characterized [27], this amounts to real-time measurement of the dressed density matrix, effecting quantum state estimation of the dressed system. [I don't like 'amounts to']. etrics for the fidelity of dynamical decoupling vary amongst platforms, and in addition to linewidth narrowing include prolonged coherence. We nominally observe a three-fold increase in the lifetime of the spectral components correspoding to the ω_{12} and ω_{23} transitions as compared with the undressed system (Fig. 3a, $1/e$ decay time 23.8(2) ms). The dressed-state coherences are expected to be greater, but were limited here to $\sim$ 100 ms by probe-induced photon scattering; admitting a lower signal-to-noise ratio using less perturbative probe [25] would permit even longer coherences to be revealed. o appraise the success of decoupling of the dressed state transitions, and their dependence on the quadratic shift q_R, we varied the magnetic field over a wider range than was furnished by our power line noise of Fig. 2, by sweeping the bias magnetic field along z over a range $B_{\rm rf}$ [What is this B_{rf}!?] during the measurement interval. [We should tread lightly here on this previous comment. We should avoid drawing attention to the question "If it is optimally decoupled, then it should show the longest decoherence time. Have you done this?"] The control field $B_z(t) = B_0 + \alpha t + B_{\rm line}(t)$, where $\alpha = 128\,\text{mG/s}$ is the linear sweep rate; the resulting detuning variation is of order 2Ω (*cf.* the domain of Fig. 1). For each realization (or 'shot') of the experiment, we calibrate $B_z(t)$ using magnetometry of the bare Zeeman states: an rf $\pi/2$-pulse (rather than continuous coupling) initiates Larmor precession of the collective spin in the x–y plane, and the Faraday signal is composed of two tones at $\omega_\pm = \omega_L \pm q$, the bare Zeeman splittings (Fig. 3, top). For $q\,\tau_f \geq 2\pi$, where τ_f is

TABLE I. Upper sidebands of the carrier (at $\omega_{\rm rf}$) of the Faraday rotation signal $\propto \langle \hat{F}_x \rangle$ of an arbitrary dressed state superposition driven on resonance ($\Delta = 0$). Frequency and phase are reported relative to the carrier, along with the transition that each sideband corresponds to. For the initial state $|\psi(t=0)\rangle = |m_z = -1\rangle$, the sideband frequencies and amplitudes can be concisely expressed in terms of the dressed Larmor frequency ω_D and quadratic shift q_D. For each upper sideband, there is a lower sideband of the same amplitude, relative frequency and opposite relative phase. [Note removal of curlies and fracbracks in cols 4 and 5 resp of table to reduce symbology. Debatable!]

transition	frequency	$\omega_{ij} - \omega_{\rm rf}$ ($\Delta = 0$)	amplitude ($\Delta = 0$)	amplitude ($\Delta = 0$, $\lvert m_z = -1\rangle$)
(carrier)	$\omega_{\rm rf}$	0	$(\langle 3\lvert\hat{F}_x\rvert 3\rangle - \langle 1\lvert\hat{F}_x\rvert 1\rangle)(\rho_{33} - \rho_{11})$	$q_D\Omega/2\omega_D^2$
$\lvert 1\rangle \leftrightarrow \lvert 2\rangle$	$\omega_{\rm rf} + \omega_{12}$	$\omega_D + q_D$	$-2i\langle 1\lvert\hat{F}_y\rvert 2\rangle \mathrm{Re}\rho_{12} = -2\langle 2\lvert\hat{F}_z\rvert 3\rangle \mathrm{Re}\rho_{12}$	$\Omega/4\omega_D$
$\lvert 2\rangle \leftrightarrow \lvert 3\rangle$	$\omega_{\rm rf} + \omega_{23}$	$\omega_D - q_D$	$2i\langle 2\lvert\hat{F}_y\rvert 3\rangle \mathrm{Re}\rho_{23} = 2\langle 1\lvert\hat{F}_z\rvert 2\rangle \mathrm{Re}\rho_{23}$	$\Omega/4\omega_D$
$\lvert 1\rangle \leftrightarrow \lvert 3\rangle$	$\omega_{\rm rf} + \omega_{13}$	$2\omega_D$	$2\langle 1\lvert\hat{F}_x\rvert 3\rangle \mathrm{Re}\rho_{13}$	$q_D\Omega/4\omega_D^2$

the length of the spectrogram window, the two tones are spectrally resolved and their mean and difference yields the instantaneous $\omega_L(t)$ and $q(t)$, respectively, ω_L is then used to find $\delta B_z(t)$ (and $\Delta(t)$) by inverting the Breit-Rabi equation [18] [28].

We measured the dressed spectrum for magnetic bias fields B_0 ranging from 3.549 to 5.568 G (applied rf frequencies $f_{\rm rf}$ from 2.493 to 3.911 MHz), with a fixed Rabi frequency of $\Omega = 2\pi \times 4.505(3)$ kHz. At each field B_0 we ensured the Rabi frequency was fixed by measuring the voltage drop across the coil at $f_{\rm rf}$ with an rf lock-in amplifier which – in concert with an impedance analyzer – could be used to ensure the rf current in the coil and thus Ω was constant. The Rabi frequency was ultimately measured using the atoms by analyzing a subset of the dressed energy spectrum during the magnetic field sweep when $\Delta \leq 2\pi \times 100$ Hz [no need for $|\cdot|$ as we always swept up, right?]. The measured Rabi frequencies had a standard deviation $\sigma(\Omega) = 9.4$ Hz, validating the above method.

The dressed spectrum for the swept control field with resonant field $B_0 = 5.013$ G and $q_R = 0.403(2)$ is shown in Fig. 3b. The instantaneous dressed state splittings for all three transitions were predicted with no free parameters, and are plotted atop the spectrogram data, showing excellent agreement with the measured sidebands. Because $\delta B_z(t)$ is non-linear and non-monotonic in time, we use the raw time series from the calibration ($\Omega = 0$) and CoDD shots to form parametric $(\delta B_z(t), f_{ij}(t))$ data, by tracking the instantaneous peaks in each spectrogram. The sensitivity of the $|1\rangle \leftrightarrow |2\rangle$ and $|2\rangle \leftrightarrow |3\rangle$ transitions to magnetic field variations are shown in Fig. 3c. The synthetic clock transition is most insensitive; the measured [predicted] f_{12} varies by 39 Hz [26 Hz] for $0 \leq \delta B_z \leq B_{\rm rf}/4 = 3.2$ mG (Fig. 3c, inset). The corresponding normalized variation in $\omega_{12}/\Omega = 8.6 \times 10^{-3}$ [5.8×10^{-3}] across a detuning range of $0 \leq |\Delta/\Omega| \leq 0.5$. By comparison, the normalized variation at $q_R = 0$ is $(\sqrt{5} - 2)/2 \approx 0.118$; 14 [20] times higher than the observed [predicted] variation. Alternatively, the normalized variation of the $|m_z = \pm 1\rangle \leftrightarrow |m_z = 0\rangle$ Zeeman transitions at $q = 0$ is 0.5; 58 [86] times higher than the observed [predicted] variation in the synthetic clock transition frequency.

In the adiabatic limit, the dressed state populations remain constant and the above superposition evolves under phase acquisition $e^{-i\omega_i t}$ by each dressed state $|i\rangle$ [29]. We quantify the stasis of the dressed superposition using the generalized adiabatic parameter $\Gamma \equiv |\mathbf{\Omega}(t)/\dot{\theta}(t)|$, where $\mathbf{\Omega} = \mathbf{B}_{\rm eff}/\gamma \equiv \Omega\,\mathbf{e}_x + \Delta\,\mathbf{e}_x$ and $\tan\theta \equiv \Omega/\Delta$. [If using Γ must say that $\Gamma \gg 1$ means adiabatic or whatever...] For constant coupling amplitude $\dot{\Omega} = 0$, $\dot{\theta}(t) = -\Omega\dot{\Delta}(t)/|\mathbf{\Omega}|^2$. For the magnetic field sweeps used here, Γ exceeded 200 everywhere and was on average $\gtrsim 600$. Nevertheless, the continuous spectra when plotted parametrically (Fig. 3c) exhibit some evidence of non-adiabatic following. [do they?] Numerical integration of the Schrödinger equation of the known control Hamiltonian confirms that dressed state populations deviate by no more than X % from their initial values.

To test the predictive power of our measurement of dynamical decoupling, we determined the curvature of the synthetic clock transition with respect to magnetic field variations, inspecting the quadratic coefficient of a polynomial fit to $(\delta B_z, f_{12})$ data. The results of this model independent analysis are shown in Fig. 4 for q_R between 0.2 and 0.5. The curvature $\partial^2 f_{12}/\partial B_z^2$ is predicted analytically to be near-linear in q_R over this range. Accordingly, we perform linear regression to the measured curvature versus q_R to infer $q_{R,\rm magic}$, where the synthetic clock transition has vanishing curvature, and find $q_{R,\rm magic}$ (expt.) $= 0.350(6)$, in agreement with the theoretical value in Eq. (1). The minimum curvature measured occured at $q_R = 0.351(2)$, with a value of $\left(\partial^2 f_{12}/\partial B_z^2\right)_{\rm min} = 1\,\mathrm{Hz/mG^2}$ [1 MHz/G^2]. In dimensionless units – with the splitting and detuning normalized to the Rabi frequency – $\left(\Omega\,\partial^2\omega_{12}/\partial\Delta^2\right)_{\rm min} = 0.02$, fifty times lower than the curvature of this transition for the second-order decoupled ($q_R = 0$) case.

Despite long coherence times, the low duty cycle ($D <$

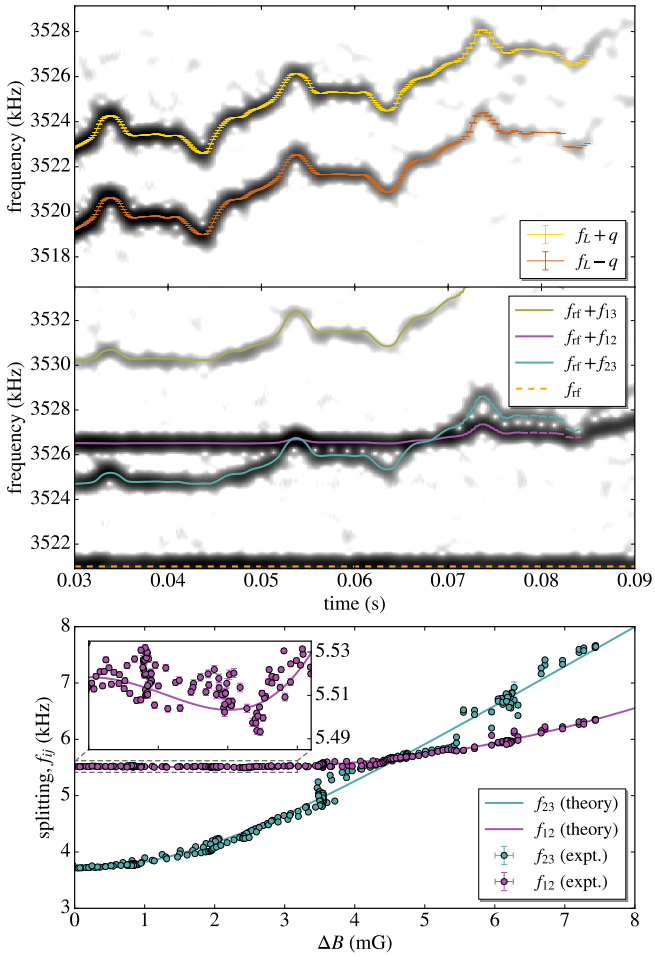

FIG. 3. Real-time CoDD observation for $q_R = 0.402(3)$. (a) and (b) are spectrograms of a continuous weak measurement of $\langle \hat{F}_x \rangle$. (a) Magnetometry of the bare Zeeman states ($\Omega = 0$) used to calibrate $B_z(t) = B_0 + \delta B_z(t)$ over the interrogation interval, in which the field [detuning] varies over a range $\sim B_{\rm rf}$ [2Ω]. We numerically track the bare Zeeman splittings (gold/orange) to determine the instantaneous Larmor frequency $f_L(t)$ and quadratic shift $q(t)$. (b) The field is swept over the same range but the rf dressing is applied ($\Omega > 0$). Three sidebands above (shown) and below the carrier at $f_{\rm rf} = 3.521\,$MHz (dashed, orange) reveal the dressed state splittings $f_{ij} = \omega_{ij}/(2\pi)$. (c) A parametric plot of $f_{12}(t)$ and $f_{23}(t)$ versus $\delta B_z(t)$ by combining analysis of (a) and (b). Solid curves in (b) and (c) are theoretical splittings from an eigenspectrum calculation, provided only $f_{\rm rf}$, $B_z(t)$, and Ω, i.e. no free parameters. Variation of the synthetic clock transition f_{12} for $0 \le \delta B_z \le B_{\rm rf}/4 = 3.2\,$mG (c, inset).

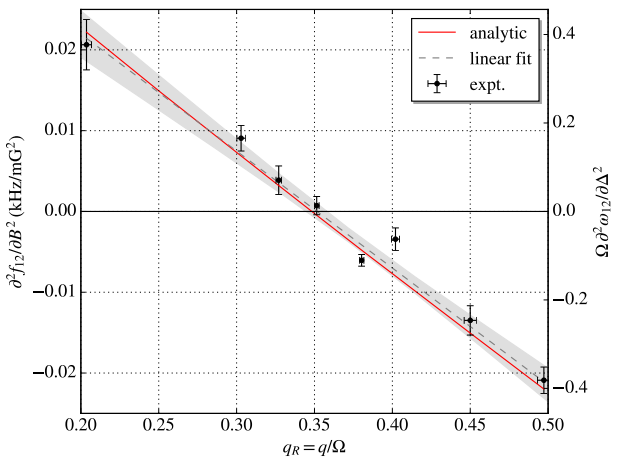

FIG. 4. Curvature of the synthetic clock transition for normalized quadratic shifts $q_R \in [0.2, 0.5]$. The measured curvature (black points) was determined from polynomial fitting to $(\delta B_z, f_{12})$ data shown in Fig. 3(c). Vertical and horizontal error bars correspond to the standard error of the regression and uncertainty in q_R (via $u(q)$ and $u(\Omega)$ at each field B_0), respectively. A linear fit (black, dashed) with 1σ confidence band (gray, shaded) are shown, whose intercept can be used to impute $q_{R,\rm magic}$ (expt.) $= 0.350(6)$. The analytic expression for the curvature (red) is consistent with the data-driven analysis of the curvature, *cf.* $q_{R,\rm magic}$ (theory) $= 0.348$. The left [right] vertical axis shows the curvature $\partial^2 f_{12}/\partial B_z^2$ [$\Omega\,\partial^2\omega_{12}/\partial\Delta^2$] in absolute units of kHz/G^2 [dimensionless units]. The normalized curvature is unity when $q_R = 0$.

0.01) and low repitition rate ($T_{\rm shot} \gtrsim 10\,$s) of cold quantum gas experiments make it challenging to achieve metrological sensitivities per unit bandwidth that are competitive with other platforms. Here $D = 0.005$ and $T_{\rm shot} = 20\,$s, yet we make many more spin projection measurements ([N_m = blah] at a shot-noise limited SNR of 10–100 [25]) than traditional cold atom experiments ($N_m = 1$ to several, e.g. absorption or dispersive imaging). This intra-shot revelation of the time and frequency domain renders the measurement of these spectra orders of magnitude more efficient. For example, the single spectrum shown in Fig. 3 would take $\sim$ (10 shots per δB_z per ω_{ij}) $\times$ (100 δB_z values) $\times$ (3 transitions ω_{ij}) $= 3000$ shots, or $\sim 6 \times 10^4\,$s $= 1000$ minutes of data acquisition. We acquire this spectrum in a single shot, i.e. 20 s. The data used to generate Fig. 4 was acquired in only 5 minutes.

In summary, we have demonstrated real-time measurement of continuous dynamical decoupling in a spin-1 quantum gas, and expeditious optimization of this decoupling by varying the the relative asymmetry of the Zeeman state splittings. Continuous weak measurement via the Faraday effect yields information about the rf-dressed superposition, the dressed-state couplings and energies, simultaneously. In this measurement regime, we do not resolve the quantum noise of the decoupled collective spin. With a modification of the probe (atom-shot noise dominated) we could measure and affect the quantum noise dynamically, and probing the dressed state coherences in this regime may expose non-Gaussian quantum noise geometries in a manner analogous to Ref. [30]. Our time-frequency reduction of the weak measurement record make plain the cyclic coupling of all three dressed states, which could be applied to emulating quantum

spin ladders with frustrated interactions. By making the coupling spatially dependent, the optimal decoupling of the synthetic clock states demonstrated can be applied to critical phenomena in spin-orbit coupled spin-1 Bose gases, as $q = q_{R,\mathrm{magic}}\Omega$ traverses the polar-striped and plane-wave phases in the vicinity of a tricritical point of the (Ω, q) phase diagram [31]. Indeed the Faraday probe beam – used to detect magnetization – could constitute one of the Raman beams used to generate the spin-orbit coupling.

[1] M. J. Biercuk, H. Uys, A. P. VanDevender, N. Shiga, W. M. Itano, and J. J. Bollinger, Nature **458**, 996 (2009).

[2] G. d. Lange, Z. H. Wang, D. Ristè, V. V. Dobrovitski, and R. Hanson, Science **330**, 60 (2010).

[3] H. Bluhm, S. Foletti, I. Neder, M. Rudner, D. Mahalu, V. Umansky, and A. Yacoby, Nature Physics **7**, 109 (2011).

[4] F. F. Fanchini, J. E. M. Hornos, and R. d. J. Napolitano, Physical Review A **75**, 022329 (2007).

[5] M. Hirose, C. D. Aiello, and P. Cappellaro, Physical Review A **86**, 062320 (2012).

[6] M. Loretz, T. Rosskopf, and C. L. Degen, Physical Review Letters **110**, 017602 (2013).

[7] J.-M. Cai, B. Naydenov, R. Pfeiffer, L. P. McGuinness, K. D. Jahnke, F. Jelezko, M. B. Plenio, and A. Retzker, New Journal of Physics **14**, 113023 (2012); J. Cai, F. Jelezko, N. Katz, A. Retzker, and M. B. Plenio, New Journal of Physics **14**, 093030 (2012).

[8] D. A. Golter, T. K. Baldwin, and H. Wang, Physical Review Letters **113**, 237601 (2014).

[9] N. Aharon, M. Drewsen, and A. Retzker, Physical Review Letters **111**, 230507 (2013).

[10] P. Facchi and S. Pascazio, Physical Review Letters **89**, 080401 (2002); P. Facchi, D. A. Lidar, and S. Pascazio, Physical Review A **69**, 032314 (2004).

[11] R. Vijay, C. Macklin, D. H. Slichter, S. J. Weber, K. W. Murch, R. Naik, A. N. Korotkov, and I. Siddiqi, Nature **490**, 77 (2012).

[12] A. Valdés-Curiel, D. Trypogeorgos, E. E. Marshall, and I. B. Spielman, New Journal of Physics **19**, 033025 (2017).

[13] C. F. Ockeloen, R. Schmied, M. F. Riedel, and P. Treutlein, Physical Review Letters **111**, 143001 (2013); A. Horsley and P. Treutlein, Applied Physics Letters **108**, 211102 (2016).

[14] D. M. Stamper-Kurn and M. Ueda, Reviews of Modern Physics **85**, 1191 (2013).

[15] H.-J. Mikeska and A. K. Kolezhuk, in *Quantum Magnetism*, Lecture Notes in Physics No. 645, edited by U. Schollwöck, J. Richter, D. J. J. Farnell, and R. F. Bishop (Springer Berlin Heidelberg, 2004) pp. 1–83.

[16] E. Majorana, Il Nuovo Cimento (1924-1942) **9**, 43 (1932).

[17] J. M. Boss, K. S. Cujia, J. Zopes, and C. L. Degen, Science **356**, 837 (2017); S. Schmitt, T. Gefen, F. M. Stürner, T. Unden, G. Wolff, C. Müller, J. Scheuer, B. Naydenov, M. Markham, S. Pezzagna, J. Meijer, I. Schwarz, M. Plenio, A. Retzker, L. P. McGuinness, and F. Jelezko, Science **356**, 832 (2017).

[18] N. Ramsey, *Molecular beams* (Clarendon Press, 1956).

[19] F. Gerbier, A. Widera, S. Fölling, O. Mandel, and I. Bloch, Physical Review A **73**, 041602 (2006).

[20] G. A. Smith, S. Chaudhury, A. Silberfarb, I. H. Deutsch, and P. S. Jessen, Physical Review Letters **93**, 163602 (2004).

[21] The curvature of the dressed-state energies is evaluated using perturbation theory. In particular, the dimensionless curvature of ω_{12} is $\partial^2(\omega_{12}/\Omega)/\partial(\Delta/\Omega)^2 = \Omega\,\partial^2\omega_{12}/\partial\Delta^2 = -(3q_R\sqrt{4+q_R^2} - q_R^2 - 2)/(2\sqrt{4+q_R^2})$. For $q_R = 0$, we recover the spin-1/2 result, $\Omega\,\partial^2\omega_{12}/\partial\Delta^2 = 1$.

[22] The curvature of the dressed-state energies is evaluated using perturbation theory. In particular, the dimensionless curvature of ω_{12} is $\partial^2(\omega_{12}/\Omega)/\partial(\Delta/\Omega)^2 = \Omega\,\partial^2\omega_{12}/\partial\Delta^2 = -(3q_R\sqrt{4+q_R^2} - q_R^2 - 2)/(2\sqrt{4+q_R^2})$. For $q_R = 0$, we recover the spin-1/2 result, $\Omega\,\partial^2\omega_{12}/\partial\Delta^2 = 1$.

[23] We take $\Delta = -\gamma\,\delta B_z$ for $|\Delta| \leq 2\Omega$ ($|\delta B_z| \leq B_{\mathrm{rf}}/2$) and $|\partial q/\partial\Delta| \approx |\gamma^{-1}\partial q/\partial B_z| = |2B_z q_Z/\gamma| \ll 1$, valid to 10^{-3} for the field strengths $B_z \lesssim 5\,\mathrm{G}$ used here, resulting in vanishing third-order derivatives of ω_i with respect to detuning. In general, the variation of q with Δ (or δB_z) can be accounted for using the Breit-Rabi equation, leading to a residual linear and cubic variation of ω_{12} with δB_z, and a small correction to $q_{R,\mathrm{magic}}$ in Eq. (1).

[24] A. A. Wood, L. M. Bennie, A. Duong, M. Jasperse, L. D. Turner, and R. P. Anderson, Physical Review A **92**, 053604 (2015).

[25] M. Jasperse, M. J. Kewming, S. N. Fischer, P. Pakkiam, R. P. Anderson, and L. D. Turner, arXiv:1705.10965 (2017).

[26] Y. Liu, S. Jung, S. E. Maxwell, L. D. Turner, E. Tiesinga, and P. D. Lett, Physical Review Letters **102**, 125301 (2009); G. A. Smith, A. Silberfarb, I. H. Deutsch, and P. S. Jessen, Physical Review Letters **97**, 180403 (2006).

[27] N. Lundblad and I. B. Spielman, arXiv:1706.xxxxx (2017).

[28] The experiment is synchronized to the mains power line; the harmonic composition of which varies little between contiguous shots (20 s apart), and thus the measured $\delta B_z(t)$ and $q(t)$ from the calibration [fiducial?] shot serve as a good proxy for the values experienced by the atoms in the subsequent decoupled shot.

[29] A. Messiah, *Quantum mechanics*, Vol. 2 (North-Holland, 1962).

[30] G. Colangelo, F. M. Ciurana, L. C. Bianchet, R. J. Sewell, and M. W. Mitchell, Nature **543**, 525 (2017).

[31] G. I. Martone, Physical Review Letters **117** (2016), 10.1103/PhysRevLett.117.125301.

[32] M. R. Matthews, Physical Review Letters **81**, 243 (1998).

[33] M. F. Riedel, P. Böhi, Y. Li, T. W. Hänsch, A. Sinatra, and P. Treutlein, Nature **464**, 1170 (2010).

[34] C. Gross, T. Zibold, E. Nicklas, J. Estève, and M. K. Oberthaler, Nature **464**, 1165 (2010).

[35] M. Kitagawa and M. Ueda, Physical Review A **47**, 5138 (1993).

[36] I. D. Leroux, M. H. Schleier-Smith, and V. Vuletić, Physical Review Letters **104**, 073602 (2010).

[37] S. Chaudhury, G. A. Smith, K. Schulz, and P. S. Jessen, Physical Review Letters **96**, 043001 (2006).

[38] A. Kuzmich, L. Mandel, J. Janis, Y. E. Young, R. Ejnisman, and N. P. Bigelow, Physical Review A **60**, 2346

(1999).
[39] A. Kuzmich, L. Mandel, and N. P. Bigelow, Physical Review Letters **85**, 1594 (2000).
[40] H. J. Lipkin, N. Meshkov, and A. J. Glick, Nuclear Physics **62**, 188 (1965).
[41] W. Muessel, H. Strobel, D. Linnemann, T. Zibold, B. Juliá-Díaz, and M. K. Oberthaler, Phys. Rev. A **92**, 023603 (2015).
[42] S. T. Merkel, C. A. Riofrío, S. T. Flammia, and I. H. Deutsch, Physical Review A **81**, 032126 (2010).
[43] A. A. Wood, L. D. Turner, and R. P. Anderson, Physical Review A **94**, 052503 (2016).

Notes

Literature review

- Minimally sensitive states in other systems, e.g. $|F = 1, m = -1\rangle \leftrightarrow |F = 2, m = +1\rangle$ at $B = 3.23\,\mathrm{G}$ [32], clocks.

✓ Wide utility of these states for clocks, magnetometers (including microwave, e.g. Treutlein [13]), quantum information, and quantum emulation, e.g. elusive many-body spin-singlet state which requires unforgiving field stability [14].

✓ In electronically/magnetically sensitive spin experiments, magnetic field noise manifest as small perturbations $\Delta\hat{F}_z$ which shift the energy eigenvalues.

- Continuous measurement of an $F = 1$ system using the Faraday effect necessitates the state be magnetically sensitive $\langle\hat{F}_x\rangle \neq 0$ but dark states [incorrect use of dark states?], protected from magnetic field fluctuations only exist in the nullspace of $\hat{F}_z$ i.e. $\hat{F}_z|\psi\rangle = \hat{0}$ [9]. Therefore, no state exists which is both insensitive to magnetic fields fluctuations and capable of generating a continuous Faraday signal; the two are not mutually exclusive.

- Whereas the aim of a protected qubit subspace is to create *states* that are insensitive to fields, the impetus of metrology is to create *superpositions* and *transitions* insensitive to fields.

✓ Continuous dynamical decoupling (CoDD) [4, 10] occurs when the spin undergoes rotations in a plane perpendicular induce perturbation, i.e $\hat{F}_x$ or $\hat{F}_x$ most readily achieved through Rabi coupling where $\Omega \gg \delta B$.

✓ Decoupling can be used to increase the coherence time of single qubits [8] which can be extended even further by doubly dressing the system and decoupling from noise induced by the first coupling field [7] (concatenated continuous decoupling, or CCD).

- It has also been shown theoretically that CoDD is superior than pulsed sequence dynamical decoupling for single solid-state qubits for magnetometery [5].

✓ Motivate continuous measurement, especially in context of measurement bandwidth; it doesn't make sense to measure something in kHz–MHz band using a shot-based (0.1 Hz or less) readout. Why? Can't react, can't feedback, can't always assume periodicity/repeatability.

- Whilst the paper is not focused on introducing spectrograms, we can say they provide a new mechanism for appraising spectrum of a quantum system in real-time.

- From a magnetometry perspective, breaking rotational symmetry is bad because you want there to be no anisotropy to the sensitivity. How does this relate to this work?

✓ (How) The $\hat{F}_z^2$ interaction has been controlled using static magnetic fields, microwave ac Stark shifts [19] and tensor-light shifts of off-resonant electric dipole transitions [20], respectively. In collective pseudo-spins, it can arise from nonlinear collisional interactions [33, 34].

- (What) This nonlinear term has been used to traverse the magnetic phase space of a spinor quantum gas, drive quantum quenches of same, initiate spin dynamics in optical lattices [19], enact the canonical spin-squeezing of Kitagawa and Ueda [35]: one-axis twisting (shear of coherent spin state uncertainty region) that has squeezed atomic spins in cavities [36], Bose-Einstein condensates [33, 34], and superconducting qubits.

Continuous measurement using the linear Faraday effect:

✓ Paramagnetic Faraday effect has been used to continuously measure spin-mixing dynamics of a polar spinor condensate [26].

✓ Quantum state tomography (QST) [20, 26] using continuous weak measurement and dynamical control. Ref. [20, 2004] foreshadows "real-time estimation of the spin density matrix" via weak measurement.

- Real-time nonperturbing polarization probe (tensor-based at $\Delta \sim \Delta_{HF}$, not Faraday) in Ref. [37] measured hyperfine Rabi oscillations of the collective clock-transition pseudospin. The birefringence is modulated near baseband, i.e. polarization rotation oscillates at the Rabi frequency. This paper highlights the fact that "atoms in $m_F = 0$ clock states cannot contribute to Faraday rotation, and therefore in the limit $\Delta \gg \Delta_{HF}$ the probe polarization does not couple to the clock pseudospin". In contrast, the synthetic clock states presented here can yield Faraday rotation, including in the $\Delta \gg \Delta_{HF}$ limit. Moreover, the probe-induced differential light shift changed the resonance of the clock-transition (detected as a modified total Rabi frequency). Also from this paper:

> ...if a measurement can resolve the quantum fluctuations associated with a

collective observable, then backaction will be induced on the collective state and the observable can be squeezed.

- Faraday QND measurement of collective spin projection of an atomic beam as a way of preparing squeezed spin states [38, 39]. This is an odd regime where the background field is modulated faster than the peak Larmor frequency, but it is a rare example of the polarimetry signal being fed to a spectrum analyzer/lock-in detector.

Other exotica:

- Spin-orbit coupled spin-1 Bose gases exhibit e.g. tricriticality in (Ω, q) phase diagrams [31], where the optimal decoupling $q = q_{R,\mathrm{magic}}\Omega$ is a line traversing multiple phases, in the vicinity of a tricritical point of polar-striped and plane-wave phases. Although here the wavevector of the coupling is zero, the essential results may carry over, and the Faraday probe – used to detect magnetization – could constitute one of the Raman beams used to generate the spin-orbit coupling.

- Lipkin-Meshkov-Glick Hamiltonian [40] (see Refs. [16] of [41]).

Background theory

Quasi-static field along z, coupling field along x:

$$\begin{aligned}\hat{H}_{\mathrm{lab}} &= -\omega_L\hat{F}_z + q\hat{F}_z^2 + 2\Omega\cos(\omega_{\mathrm{rf}}t)\hat{F}_x\\ \Rightarrow \hat{H}_{\mathrm{rwa}} &= \Delta\hat{F}_z + q\hat{F}_z^2 + \Omega\hat{F}_x\,,\ \text{where}\\ \omega_L(B) &\equiv (E_{m=-1} - E_{m=+1})/2\hbar\,,\ \text{and}\\ q(B) &\equiv (E_{m=+1} + E_{m=-1} - 2E_{m=0})/2\hbar\end{aligned}$$

are the Larmor frequency and quadratic shift, respectively, which can be gleaned from the Breit-Rabi equation. The rf Rabi frequency $\Omega = \gamma B_{\mathrm{rf}}/2$ and detuning $\Delta(B) = \omega_{\mathrm{rf}} - \omega_L(B)$.

- At low magnetic field strengths, $\omega_L \propto B_z$ and $q \propto B^2$, and for our parameters we are justified in taking $\omega_L = \gamma B$ and $q = q_Z B_z^2$, where $\gamma = 2\pi \times 702.379\,\mathrm{kHz/G}$ is the gyromagnetic ratio for ^{87}Rb $F = 1$ and $q_Z = 2\pi \times 71.89\,\mathrm{Hz/G^2}$ the quadratic Zeeman coefficient.

✓ For most of the analysis presented here (with ω_L and q defined as above) these proportionalities need not be met, or the results, e.g. value of q_{magic} require a small correction.

- For $q = 0$, $\hat{H}_{\mathrm{lab}}$ and $\hat{H}_{\mathrm{rwa}} \propto \mathbf{B}\cdot\hat{\mathbf{F}}$ and are thus a generator of rotations, but $q\hat{F}_z^2 \neq 0$ breaks the SU(2) symmetry and $\langle\hat{\mathbf{F}}\rangle^2$ is not preserved.

- This broken symmetry lifts the degeneracy of the dressed state splittings making them distinguishable in our spectrogram measurements.

- Moreover, $\hat{H}_{\mathrm{rwa}}$ meets the requirements of reconstructing pure $SU(2F+1)$ states from a weak measurement of $\langle\hat{F}_x\rangle$ [42]; thus one can use the measurement record for quantum state estimation, but the spectrogram is similarly rich in Hamiltonian and density matrix information.

Lab frame eigenstates:

✓ Mean splitting ω_L; quadratic shift q.

✓ Pairwise coupling between $|m=-1\rangle \leftrightarrow |m=0\rangle$ and $|m=0\rangle \leftrightarrow |m=+1\rangle$ via $\hat{F}_x$ and/or $\hat{F}_y$, i.e. affected by fields transverse to the static field oscillating near ω_L.

- The $F = 1$ spin operators in the undressed basis do not span all of SU(3), i.e. $\sigma_x = (\lambda_1+\lambda_6)/\sqrt{2}$, $\sigma_y = (\lambda_2+\lambda_7)/\sqrt{2}$, and $\sigma_z = (\lambda_3+\sqrt{3}\lambda_8)/2$ (λ_4 and λ_5 which include off diagonal terms in rows/columns 1 and 3 are absent) where $\lambda_i, i = 1,\ldots,8$ are the Gell-Mann matrices.

Dressed states:

✓ Dressed Larmor frequency:

$$\begin{aligned}\omega_D &\equiv (\omega_3 - \omega_2)_{\Delta=0}/2 = (\omega_{12} + \omega_{23})_{\Delta=0}/2\\ &= \sqrt{\Omega^2 + q_D^2}\,.\end{aligned}$$

✓ Dressed quadratic shift:

$$\begin{aligned}q_D &\equiv (\omega_3 + \omega_1 - 2\omega_2)_{\Delta=0}/2\\ &= (\omega_{23} - \omega_{12})_{\Delta=0}/2\\ &= -q/2\,.\end{aligned}$$

- Thus $\Omega = \sqrt{\omega_{12}\omega_{23}}_{\Delta=0}$ and $q_D = (\omega_{23}-\omega_{12})_{\Delta=0}/2$, both of which can be attained from the dressed sideband splittings on resonance. Such high-bandwidth measurement of Ω (magnetic field oscillating along x with amplitude B_{rf} and frequency ω_L) allows (in principle) closed-loop control of Ω using the atoms.

✓ For $q = 0$ (low-field limit), the dressed states at $\Delta = 0$ are eigenstates of $\hat{F}_x$, *viz.* $|m_x = -1, 0, +1\rangle \equiv |1\rangle$, $|2\rangle$, and $|3\rangle$ respectively. (i) the spectrum has vanishing linear sensitivity to magnetic fields, with the leading quadratic sensitivity (as in spin-1/2) of the degenerate $|1\rangle \leftrightarrow |2\rangle$ and $|2\rangle \leftrightarrow |3\rangle$ transitions, and (ii) fields along y or z oscillating near the Rabi frequency Ω drive transitions between different $|m_x\rangle$ states. [Cite other dressed-ception papers on both of these.]

✓ The $F = 1$ spin operators in the resonantly dressed basis span more of SU(3), as $[\hat{F}_x]_D = (q_D/\omega_D)Q_{x^2-y^2} - (\Omega/\omega_D)\sigma_z = (q_D/\omega_D)\lambda_4 - \Omega/\omega_D(\lambda_3 + \sqrt{3}\lambda_8)/2$, $[\hat{F}_y]_D$ is a sum of λ_1, λ_2, and λ_7, and $[\hat{F}_z]_D$ is a sum of λ_1 and λ_6. The presence of $Q_{x^2-y^2} = \lambda_4$ for $q \neq 0$ signifies the coupling of dressed states $|1\rangle$ and $|3\rangle$, i.e. a non-zero $\langle 1|\hat{F}_x|3\rangle$. [The spin operators have no projection onto λ_5, even for an rf field oscillating along y.]

✓ *Transitions between dressed states:* $|1\rangle \leftrightarrow |2\rangle$ and $|2\rangle \leftrightarrow |3\rangle$ driven by fields oscillating along y or z near frequencies $\omega_D \mp q_D$, respectively. Alternatively, $|1\rangle \leftrightarrow |3\rangle$ driven by fields oscillating along x near frequency $2\omega_D$. This is very different to the fully polarized bare states $|m = \pm 1\rangle$, which are coupled by a single-photon transition as this would conserve neither photon number nor angular momentum. There is no such restriction on the dressed states however as they are neither eigenstates of $\hat{F}_z$ nor photon number.

- To drive the $|1\rangle \leftrightarrow |2\rangle$ transition exclusively (remain in the $\{|1\rangle, |2\rangle\}$ subspace) with an oscillating field along y or z, the concatenated coupling strength must be $\ll q_D$, the separation of the two-lowest dressed state transitions. This sets the *dynamic range* of ac magnetometry using the synthetic clock states alone.

✓ Curvature of the dressed-state energies can be evaluated using perturbation theory;

$$\frac{\partial^2 \omega_n}{\partial \Delta^2} = \sum_{k \neq n} \frac{|\langle k|\hat{F}_z|n\rangle|^2}{\omega_n - \omega_k} .$$

✓ Thus the curvature of the dressed-state splittings can be found. In particular, the dimensionless curvature of ω_{12} is (presuming $|\partial q/\partial \Delta| \ll 1$)

$$\begin{aligned}\frac{\partial^2(\omega_{12}/\Omega)}{\partial(\Delta/\Omega)^2} &= \Omega \frac{\partial^2 \omega_{12}}{\partial \Delta^2} \\ &= -\frac{3q_R\sqrt{4+q_R^2} - q_R^2 - 2}{2\sqrt{4+q_R^2}} .\end{aligned}$$

This vanishes when $q = q_{R,\mathrm{magic}}$, given by

$$q_{R,\mathrm{magic}} = \sqrt{(3\sqrt{2}-4)/2} \approx 0.348 .$$

For $q_R = 0$, we recover the spin-1/2 result, $\Omega\, \partial^2 \omega_{12}/\partial \Delta^2 = 1$.

✓ Similarly, perturbation theory can be used to show that the third-order derivatives of ω_n with respect to detuning all vanish when $|\partial q/\partial \Delta| \approx |\gamma^{-1}\partial q/\partial B_z| \ll 1$, and thus the leading sensitivity to detuning (and thus B_z) is fourth-order.

✓ The above can be quantified by noting that $\gamma^{-1}\partial q/\partial B_z = 2B_z q_Z/\gamma \lesssim 10^{-3}$ for $B_z \lesssim 5\,\mathrm{G}$.

- This validates the choice of our phenomenological even-polynomial model for fitting to $(\delta B_z(t), \omega_{12}(t))$ data extracted from Faraday spectrograms.

- Near $q = q_{\mathrm{magic}}$, the ratio of the Rabi frequency to the Larmor frequency is approximately:

$$\begin{aligned}\frac{\Omega}{\omega_L} &= \frac{B_{\mathrm{rf}}}{B_0} \\ &\approx \frac{q_Z B_0}{\sqrt{2}\gamma\, q_{R,\mathrm{magic}}} \\ &= 2.1 \times 10^{-4} B_0 ,\end{aligned}$$

with B_0 is in Gauss. Thus for $B_0 \lesssim 5\,\mathrm{G}$, $\Omega/\omega_L \lesssim 10^{-3}$ and the rotating-wave approximation is justified.

Swept detuning measurements

- We vary the magnetic field to affect a change in the detuning of $\Delta \in [0, 2\Omega]$, the domain of Fig. 1(B).

- Variations in $B_z \mapsto B_0 + \delta B_z$ of order $B_{\mathrm{rf}} = 2\Omega/\gamma$ affect the detuning linearly, *viz.* $\Delta = -\gamma\, \delta B_z$ for $\omega_L(B_0) = \omega_{\mathrm{rf}}$ (i.e. rf is resonant when $B_z = B_0$), and do not affect q appreciably for sufficiently small field strengths.

- Indeed, our data corroborate this since we directly measure $q(B_z(t))$ during the field sweep and find that $\sigma(q)/(2\pi) = 11.7\,\mathrm{Hz}$ on average (alternatively, inferring q from ω_L via the Breit-Rabi equation gives $\sigma(q)/(2\pi) = 1.2\,\mathrm{Hz}$).

- Thus the horizontal axis Δ/Ω in Fig. 1 is a proxy for δB_z, and ω_{12} at $q = q_{\mathrm{magic}}$ has leading-order quartic sensitivity to δB_z.

- At high fields ($B \approx 30\,\mathrm{G}$) this approximation is no longer valid; $q \approx q_{\mathrm{magic}}$ varies appreciably across $\delta B_z \in [0, B_{\mathrm{rf}}]$ and ω_{12} has weak linear dependence on δB_z [27].

✓ The control field $\mathbf{B}(t \geq 0) = -B_{\mathrm{rf}} \cos(\omega_{\mathrm{rf}} t)\mathbf{e}_x + B_z(t)\mathbf{e}_z$, where $B_z(t) = B_0 + \alpha t + B_{\mathrm{ac}}(t)$ is the sum of a linear ramp and parasitic power-line magnetic noise.

✓ *On varying Ω or q to change $q_R = q/\Omega$:* For a given static magnetic field, q_R can be modified via the Rabi frequency. However, this is not what is represented in Fig. 1, as the normalization of the horizontal and vertical axes would vary for each q_R. Importantly, the insensitivity of ω_{12} to detuning

only gets better for increasing Ω in absolute terms; if the rf amplitude is unlimited, use it. However, doing so also modifies the absolute dressed state splittings on resonance, and thus the bandwidth of the dressed spin-1 as an ac magnetometer. The take home message is then: use as high an rf amplitude as you can afford (or want to tune the ac-band to), and then modify q_R via q to realize the synthetic clock states.

✓ For $0 \leq \delta B_z \leq B_{\rm rf}/4 = 3.2\,\mathrm{mG}$ ($0 \leq |\Delta/\Omega| \leq 0.5$) we observe a variation in the splitting f_{12} of 39 Hz for the data in Fig. 3, compared to the theoretical estimate of 26 Hz. These correspond to a normalized variation in ω_{12}/Ω of 8.6×10^{-3} and 5.8×10^{-3}, respectively. By comparison, the normalized variation at $q_R = 0$ is $(\sqrt{5}-2)/2 \approx 0.118$; 14 [20] times higher than the observed [predicted] variation. Alternatively, the normalized variation of the $|m=\pm1\rangle \leftrightarrow |0\rangle$ transitions at $q=0$ is 0.5; 58 [86] times higher than the observed [predicted] variation in the synthetic clock transition frequency. [Both of these comparisons depend a lot on the range of δB! They are far more impressive (theoretically) for smaller ranges.]

Faraday signal for $|m_z=-1\rangle$: The Faraday signal we detect is proportional to $\langle\hat{F}_x\rangle$ in the laboratory frame, which is given by $\langle\psi(t)|\hat{S}^\dagger\hat{F}_x\hat{S}|\psi(t)\rangle$ where $|\psi(t)\rangle = \exp(-i\hat{H}_{\rm rwa}t/\hbar)|\psi(t=0)\rangle$, and $\hat{S} = \exp(-i\omega_{\rm rf}\hat{F}_z t)$. For an initially polarized $|\psi(t=0)\rangle = |m_z=-1\rangle$ state driven on resonance, we get

$$\langle\hat{F}_x\rangle_{\rm lab} = -\frac{\Omega}{\omega_D}\cos(q_D t)\sin(\omega_D t)\sin(\omega_{\rm rf}t) - \frac{q_D\Omega}{\omega_D^2}\sin^2(\omega_D t)\cos(\omega_{\rm rf}t)\,.$$

The first term has equal-amplitude sidebands at $\pm(\omega_D \pm q_D)$ and the second term has smaller amplitude sidebands at $\pm2\omega_D$, as summarized in Table I. The ratio of the ω_{13} sideband amplitude to the ω_{12} and ω_{23}) sideband amplitudes is $q_R/\sqrt{4+q_R^2} \approx 0.197$ for $q_R = 0.402$ in Fig. 3. For the data in Fig. 2 we measure the ratio of sideband amplitudes to be 0.699 and 0.210 of the ω_{23} and ω_{13} peaks relative to the ω_{12} peak respectively.

Faraday signal for arbitrary states: Evaluating $\langle\hat{F}_x\rangle_{\rm lab}$ in the dressed basis, one can show analytically that the sideband frequencies are the dressed state splittings ω_{ij} with amplitudes proportional to the relevant dressed-state coherence $\mathrm{Re}\{\rho_{ij}\}$ where $\rho_{ij} = \langle i|\psi\rangle\langle\psi|j\rangle$. The carrier amplitude is $(\rho_{33}-\rho_{11})\Omega/\omega_D$. This explains the relative longevity of the sidebands; the transition most sensitive to detuning is ω_{13}, and thus the coherence ρ_{13} decays the fastest in the presence of detuning noise with a measured $/1e$ signal decay time of $\tau_s = 44(1)$ms from Fig. 2. Furthermore, the decay time of the ω_{12} and ω_{23} sidebands are 74(1)ms and 71(2)ms respectively. Contrasting these results to an undressed measurement decay time $\tau_s = 21(1)$, it is clear that rf dressing shields the quantum state from magnetically induced decoherence. The constant of proportionality is the coupling strength of the dressed states.

Adiabatic considerations (✓): The rf-dressing is applied non-adiabatically, and as a result we project $|m=-1\rangle$ onto the dressed basis at the initial detuning $\Delta(t=0)$ into a state

$$\begin{pmatrix}\langle1|\psi(t=0)\rangle\\ \langle2|\psi(t=0)\rangle\\ \langle3|\psi(t=0)\rangle\end{pmatrix} \approx \begin{pmatrix}\frac{1}{\sqrt{4+q_R\left(q_R+\sqrt{q_R^2+4}\right)}}\\ -\frac{1}{\sqrt{2}}\\ \frac{1}{\sqrt{4+q_R\left(q_R-\sqrt{q_R^2+4}\right)}}\end{pmatrix}$$

for $\Delta(t=0) \ll \Omega$. In the adiabatic limit, the dressed state populations remain constant and the above superposition evolves under phase acquisition $e^{-i\omega_i t}$ by each dressed state $|i\rangle$ [29]. We quantify the stasis of the dressed superposition using the generalized adiabatic parameter $\Gamma \equiv |\mathbf{\Omega}(t)/\dot{\theta}(t)|$, where $\mathbf{\Omega} = \mathbf{B}_{\rm eff}/\gamma \equiv \Omega\,\mathbf{e}_x + \Delta\,\mathbf{e}_x$ and $\tan\theta \equiv \Omega/\Delta$. For constant coupling amplitude $\dot{\Omega} = 0$, $\dot{\theta}(t) = -\Omega\dot{\Delta}(t)/|\mathbf{\Omega}|^2$. For the magnetic field sweeps used here, $\Gamma > 200$ and $\sqrt{\langle\Gamma^2\rangle}_t \gtrsim 600$ where $\langle\cdot\rangle_t$ denotes the time-average over the duration of the sweep. Nevertheless, the continuous spectra when plotted parametrically (Fig. 3c) exhibit some evidence of non-adiabatic following. This is corroborated by numerically integrating the Schrödinger equation of the known control Hamiltonian; the dressed state populations vary slowly (compared to ω_D^{-1}) but by a few percent near minima of $\Gamma(t)$, i.e. when the sweep is least adiabatic.

Apparatus

- A component of the spin (e.g. $\langle\hat{F}_x\rangle$) transverse to the static magnetic field direction (along z) rotates the polarization of an off-resonant probe beam via the paramagnetic Faraday effect.
- By tuning the probe to a magic-zero wavelength at $\lambda = 790.0\,\mathrm{nm}$, and ensuring it is linearly polarized, the probe exerts no scalar or vector light shift on the atoms.
- The former would enact a dipole force on the cloud, perturbing its total density, whereas the latter would be manifest as a fictitious magnetic field and gradient, dephasing the collective spin [43].
- Here we used a wavelength of $\lambda = 781.15\,\mathrm{nm}$ to increase the SNR with respect to the rf pickup at $f_{\rm rf}$; the measured $1/e$ decay time of calibration peaks

$\tau_s = 23.8(2)$ ms is consistent with scattering in [25] for a 10.6 mW probe with $1/e^2$ diameter of 150 µm (peak intensity $I_0 = 120.1(4)\,\mathrm{W/cm^2}$).

- We detect the Faraday rotation of the probe light using a shot-noise limited balanced polarimeter, with bandwidth up to 8 MHz, and record the signal using an AlazarTech ATS9462 digitizer (16-bit, 180 MS/s).

- The maximum Larmor frequency and thus static magnetic field we can detect Faraday rotation at is limited by the bandwidth of the detector.

- Upon applying the radiofrequency (rf) dressing field, $|\langle \hat{F}_x \rangle| > 0$ and the signature of the coupled spin-1 system is a Faraday signal frequency modulated (FM) about a carrier at the Larmor frequency.

- The frequency difference of each FM sideband from the carrier is a calibration-free measure of each dressed state splitting ω_{ij}.

Acqusition pipeline description (alternate)

Our technique directly measures all the quantities in the dressed energy eigen spectrum using sinc fitting to the spectrogram data in a two shot experiment. The first observation calibrates essential quantities of the magnetic field ($q_z, \omega_L, \frac{\partial B}{\partial t}$) Fig. 3a characterizing the horizontal axis of Fig. 1b. In the second shot, we repeat the experiment but dress the atoms with RF Fig. 3b from which we measure the energy splitting.